AIRCRAFT INTERIOR NOISE REDUCTION BY ALTERNATE RESONANCE TUNING

SEMI-ANNUAL PROGRESS REPORT FOR THE PERIOD ENDING JUNE, 1988

NASA RESEARCH GRANT NO. NAG-1-722

Prepared for: Structural Acoustics Branch
NASA Langley Research Center

Prepared by:

Dr. Donald B. Bliss
James A. Gottwald
Mark B. Gustaveson
James R. Burton, III

Department of Mechanical Engineering
and Materials Science
Duke University
Durham, North Carolina 27706

July 1988

SECTION 1. INTRODUCTION

Existing interior noise reduction techniques for aircraft fuselages perform reasonably well at higher frequencies, but are inadequate at lower frequencies, particularly with respect to the low blade passage harmonics with high forcing levels found in propeller aircraft. A method is being studied which considers aircraft fuselages lined with panels alternately tuned to frequencies above and below the frequency that must be attenuated. Adjacent panels would oscillate at equal amplitude, to give equal source strength, but with opposite phase. Provided these adjacent panels are acoustically compact, the resulting cancellation causes the interior acoustic modes to become cutoff, and therefore be non-propagating and evanescent. This interior noise reduction method, called Alternate Resonance Tuning (ART), is currently being investigated both theoretically and experimentally. This new concept has potential application for the reduction of interior noise due to the propellers in advanced turboprop aircraft as well as for existing aircraft configurations.

The ART technique is a procedure intended to reduce low frequency noise within an aircraft fuselage. A fuselage wall could be constructed of, or lined with, a series of special panels which would allow the designer to control the wavenumber spectrum of the wall motion, thus controlling the interior sound field. By judicious tuning of the structural response of individual panels, wavelengths in the fuselage wall can be reduced to the order of the panel size, thus causing low frequency interior acoustic modes to be cutoff provided these panels are sufficiently small. By cutting off the acoustic modes in this manner, a significant reduction of interior noise at the propeller blade passage harmonics should be achieved.

Current noise control treatments have already demonstrated that the mass and stiffness of individual fuselage panels can be altered. It seems reasonable, therefore, that panel resonant frequencies can be manipulated to achieve the ART effect. Application of this concept might involve the modification of existing structural panels or development of a new design for fuselage interior trim panels. Although complete acoustic cutoff will not be achievable in practice, an approximate cancellation should still substantially reduce the interior noise levels at the particular frequency of interest. It is important to note that the ART method utilizes the flexibility and dynamic behavior of the structure to good advantage, although these properties are not normally beneficial in noise control.

This progress report summarizes the work carried out at Duke University during the third six month interval of a contract supported by the Structural Acoustics Branch at NASA Langley. Considerable progress has been made both theoretically and experimentally as described in the following sections. It is important to note that all of the work carried out so far indicates the ART concept is indeed capable of achieving a significant reduction in the sound transmission through flexible walls.

SECTION 2. THEORETICAL ANALYSIS

Model problem development and analysis continues with the Alternate Resonance Tuning concept. The various topics described below are presently at different stages of completion. These topics include the following:

- investigation of the effectiveness of the ART concept under an external propagating pressure field associated with propeller passage by the fuselage;
- analysis of ART performance with a double panel wall mounted in a flexible frame model;
- development of a data fitting scheme using a branch analysis (June, 1987 progress report mass ratio optimization) with a Newton-Raphson scheme in multiple dimensions to determine values of critical parameters in the actual experimental apparatus;
- investigation of the ART effect with real panels as opposed to the spring-mass-damper systems currently used in much of the theory.

Section 2a. External Pressure Field Modelling

The high trace speed of the travelling exterior pressure disturbances caused by propeller rotation is an unavoidable effect with advanced turboprop engine/propeller designs. An initial analysis has been undertaken to investigate the effectiveness of the ART concept under this more generalized exterior pressure field. Figure 2a-1 shows the hypothetical configuration of an aircraft's exterior wall used for this analysis. A finite number of panels ($0 < j < Q$) each of height H is considered, where the panel impedances are modelled as spring-mass-damper systems with impedance given by the customary relation

$$Z_{j\ mech} = R + i(m\omega - {}^{s}/_{\omega}) \qquad 2a.1$$

The j index numbers the panels as shown in Figure 2a-1. Only two varieties of ART panels are considered in the analysis, having their resonant frequencies either above or below the desired attenuation frequency. An exterior pressure loading is assumed to be of the form

$$P_{EX} = P_E e^{i(\omega t - k_e z)} \qquad 2a.2$$

where P and k_e are the amplitude and wavenumber of the exterior forcing pressure field. The trace speed of the pressure forcing is then $c_e = {}^{\omega}/k_e$ which can be specified to be either subsonic or supersonic. Throughout the entire analysis, it is assumed that the imposed exterior pressure loading is much larger than the exterior loading associated with the acoustic response, and as

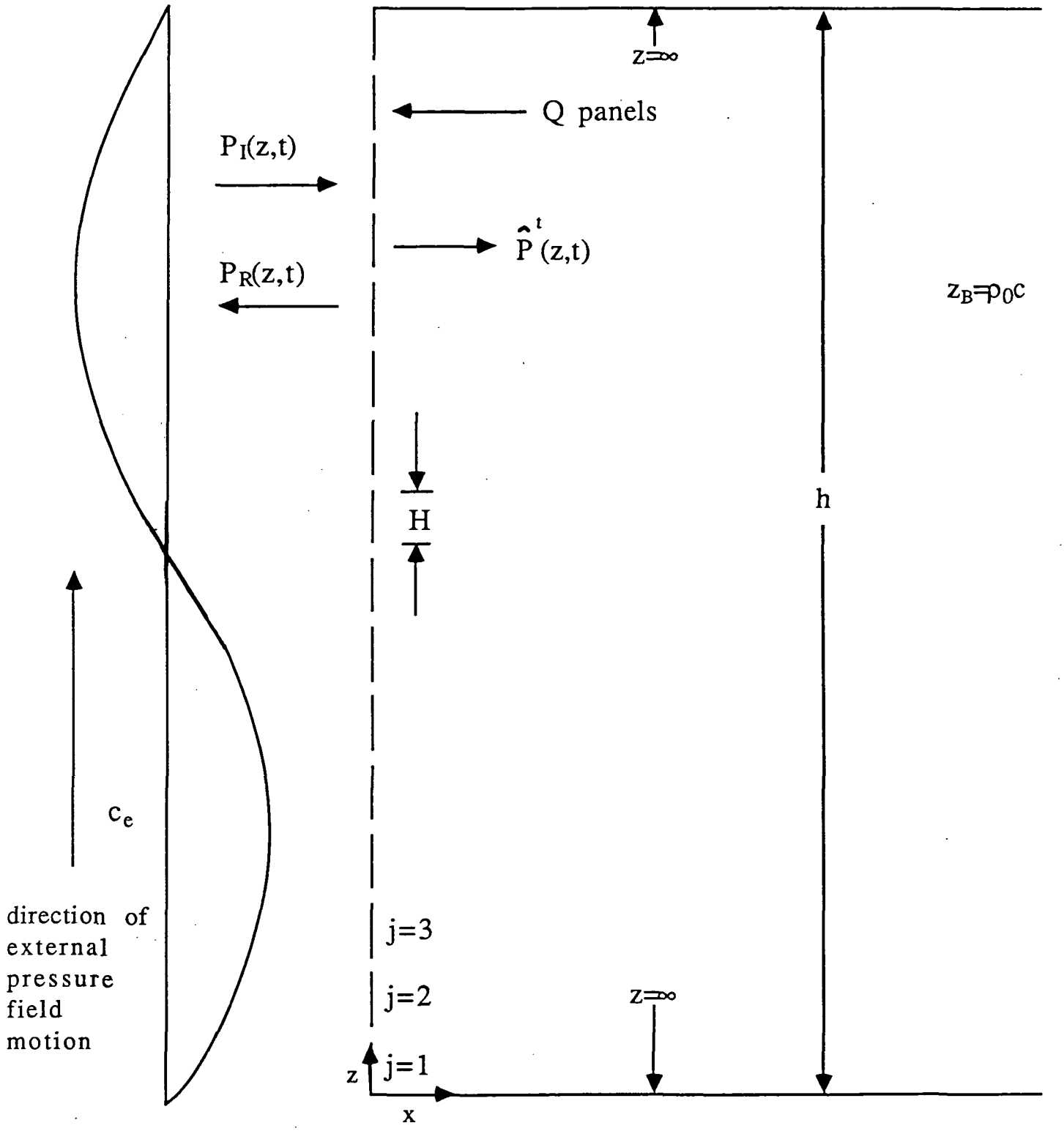

Figure 2a-1: Configuration used for analysis of travelling exterior pressure disturbance.

such, the latter will be ignored. The general interior acoustic solution for this problem is identical to the general expression for acoustic modes propagating in a duct, namely

$$P_n(x,z,t) = \sum_{n=0}^{\infty} P_n \cos\frac{n\pi z}{h} e^{i(\omega t - k_{xn}x)} \qquad 2a.3$$

and

$$k_{xn} = \sqrt{\frac{\omega^2}{c^2} - \left(\frac{n\pi}{h}\right)^2} \qquad 2a.4$$

The only boundary condition to be considered is that the velocity at the interior walls must be zero. Simple application of the vertical momentum equation

$$\frac{\partial w}{\partial t} = -\frac{1}{\rho_0}\frac{\partial p}{\partial z} \qquad 2a.5$$

via differentiation in the z direction shows that Equation 2a.3 above satisfies this requirement. The solution technique then proceeds to determine the total exterior force on the jth panel by integrating the exterior hydrodynamic loading (Equation 2a.3 above) over appropriate limits as shown below.

$$F_{j_{x=0-}} = \int_{(j-1)H}^{jH} P_E e^{i(\omega t - k_e z)} dz \qquad 2a.6$$

Similarly, the total interior force over the jth panel may be obtained by integrating Equation 2a.3 over similar limits at x = 0. The net force acting on the panels is thus given by the difference of these interior and exterior forces. Application of mechanical impedance then relates panel velocity and net force through the relation

$$F_{x=0+} - F_{x=0-} = F_{j\,net} = u_j Z_{j\,mech} \qquad 2a.7$$

The linearized horizontal momentum equation

$$\frac{\partial u}{\partial t} = -\frac{1}{\rho_0}\frac{\partial p}{\partial x} \qquad 2a.8$$

can then be used to further relate velocity and pressure. Substitution of Equation 2a.6 into Equation 2a.7 and 2a.8 then yields an expression which contains interior acoustic pressure as a function of all system parameters. Note that this analysis includes the coupling of the interior acoustic loading and the panel motion. Extensive manipulation involving the application of orthogonality and appropriate nondimensionalization of the results leads to a set of linear algebraic

equations which may be solved for the coefficients of the interior acoustic solution Equation 2a.3 above. The order of this linear algebraic system is consistent with the desired number of acoustic modes assumed in the solution.

The analytical work with this problem has been completed, and a computer program is currently being debugged.The system can be solved with any even number of panels (since ART panels are designed in pairs) and any number of acoustic modes. Figure 2a-2 shows a preliminary solution for the magnitude of the first pressure coefficient of Equation 2a.3 above as a function of nondimensionalized pressure. The results shown in Figure 2a.2 are expressed as a ratio of the first ART panel coefficient normalized by the first identical panel coefficient. The ART design frequency is arbitrarily chosen as 3.0, with individual panel resonances set at 2.5 and 3.5. The damping ratio was assumed to be 0.01, and the wavelength of the external pressure disturbance is long compared to a single panel height. The first ART panel is given a mass value of 1.0; the second ART panel is assigned a mass value of 0.6. These two mass values are the mass ratios (ignoring surrounding air mass) found using the mass ratio code developed last year for the duct panel models to place the ART cancellation frequency halfway between the panel resonance frequencies. The surrounding apparent mass causes some deviation from the design frequency. The hydrodynamic terms are especially important near the panel resonance frequencies. Most notable, however, is the large reduction in the magnitude of the first pressure coefficient around the ART design frequency, indicating the effectiveness of the ART treatment. A topic of continuing investigation here is the relationship of the masses of the panels. The high and low frequency limits can be easily explained for Figure 2a-2 using an application of the mass and stiffness laws with the given system parameters. For the high frequency limit, neglecting the stiffness and resistance terms in Equation 2a.1 yields the following simplified mass law for both identical and ART panels

$$Z_{high\ \omega} = \frac{P}{U} \, im\omega \qquad 2a.9$$

For both ART and identical panels, a ratio can be constructed of the form

$$\frac{P_{0\ ART}}{P_{0\ IDEN}} = \left(\frac{1}{m_{1\ ART}} + \frac{1}{m_{2\ ART}}\right) \Big/ \left(\frac{1}{m_{1\ IDEN}} + \frac{1}{m_{2\ IDEN}}\right) \qquad 2a.10$$

Substitution of the individual panel parameter values into Equation 2a.10 above yields the appropriate high frequency limit. A similar procedure will yield a similar low frequency limit. The example demonstrates the important role played by the mass ratios in the ART effect, and more attention will be devoted to understanding and optimizing the behavior of this important parameter.

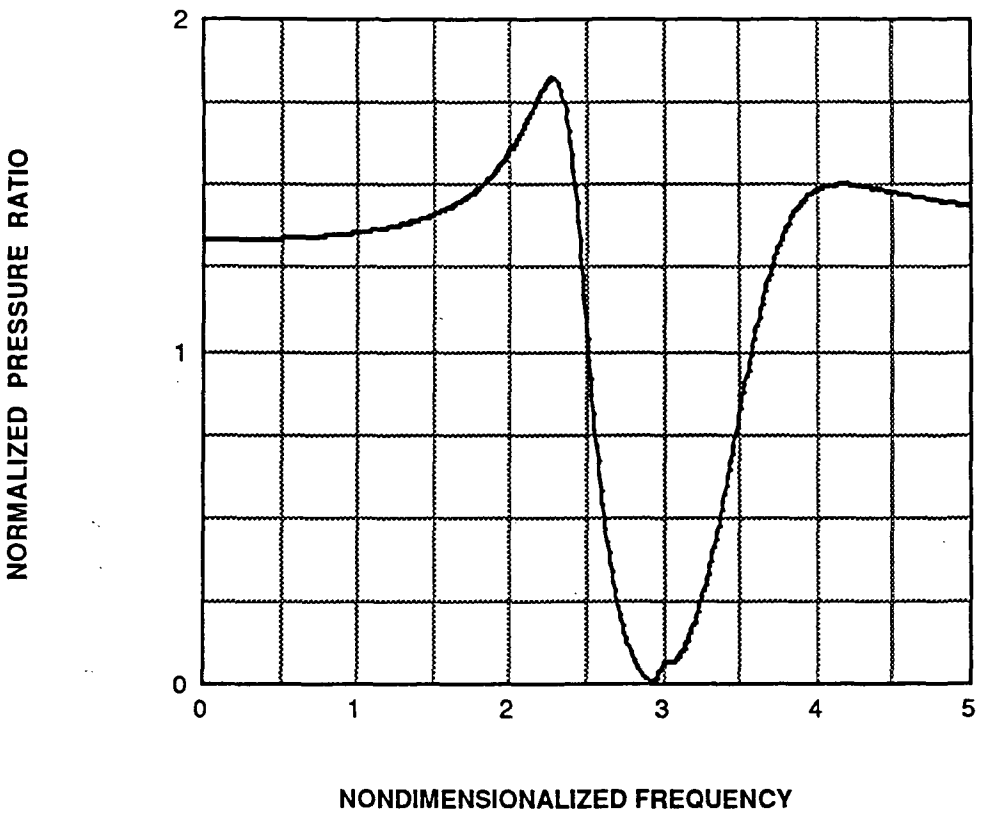

Figure 2a-2: Magnitude of the first ART panel pressure coefficient normalized with magnitude of first identical panel pressure coefficient.

Section 2b. Double Panel Wall and Flexible Frame Development

Initial analytic work has been completed on a double wall model with four panels on each wall attached to a flexible frame. The parameters in this model can be adjusted to represent a number of systems. This model, shown schematically in Figure 2b-1, consists of panel masses tied to a movable frame via springs and dampers. The effective airspring and inertial loading associated with the air space between the walls is also being modelled. The steps required to derive the governing equations for this system are essentially the same as those outlined in the August, 1987 progress report, although considerably more work is required. This system can also model the double panel wall experiments presented in Section 3c of the present report.

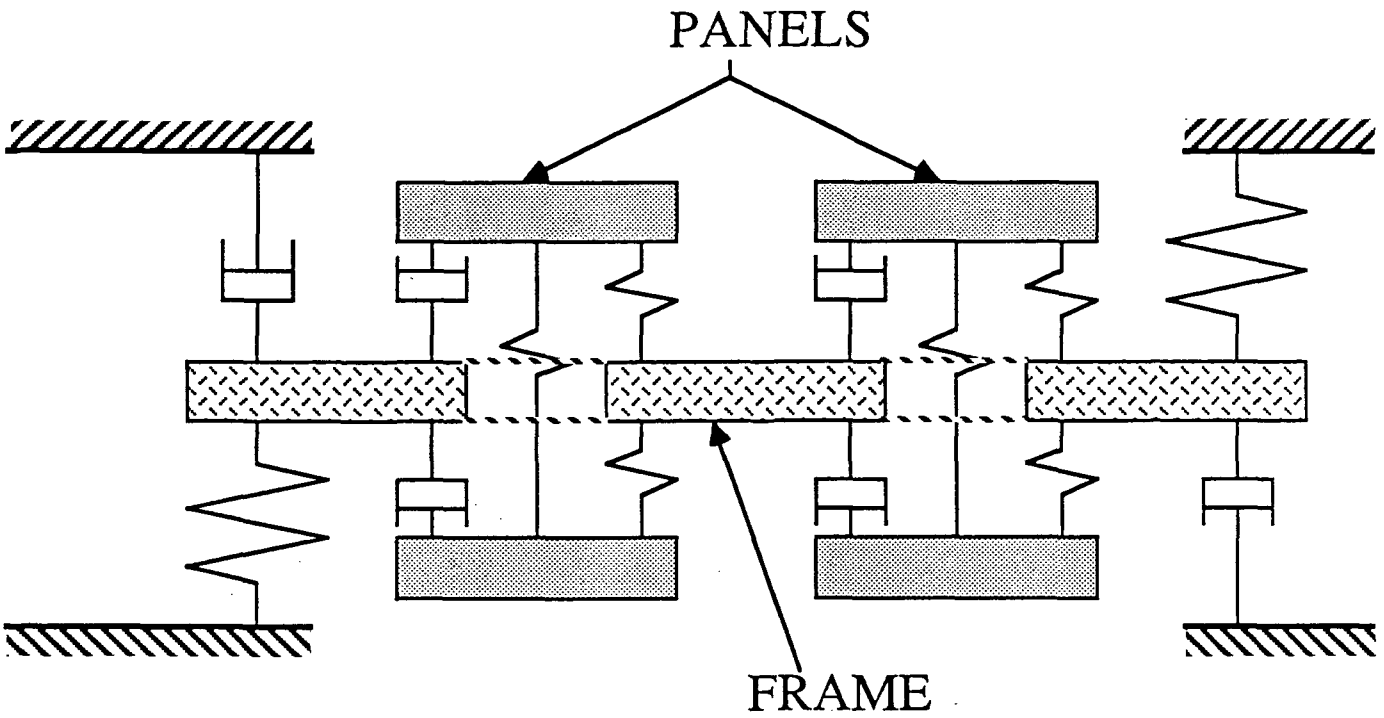

Figure 2b-1: Flexible Frame Model

Section 2c. Newton-Raphson Data Fitting Technique

Initial work has also begun on a data fitting program designed to use real ART transmission loss data to determine the values of some of the nondimensional parameters used in the analyses. A trial-and-error curvefit to an older set of data is shown in Figure 2c-1. The panel resonances for this dataset are at approximately 100 Hz and 300 Hz, and the termination is anechoic. It is anticipated that a better understanding of the interaction of the current set of nondimensionalized parameters will be gained through the use of this program. Alternatively, the results of this analysis may suggest new sets of more effective parameters to achieve a stronger ART cancellation effect.

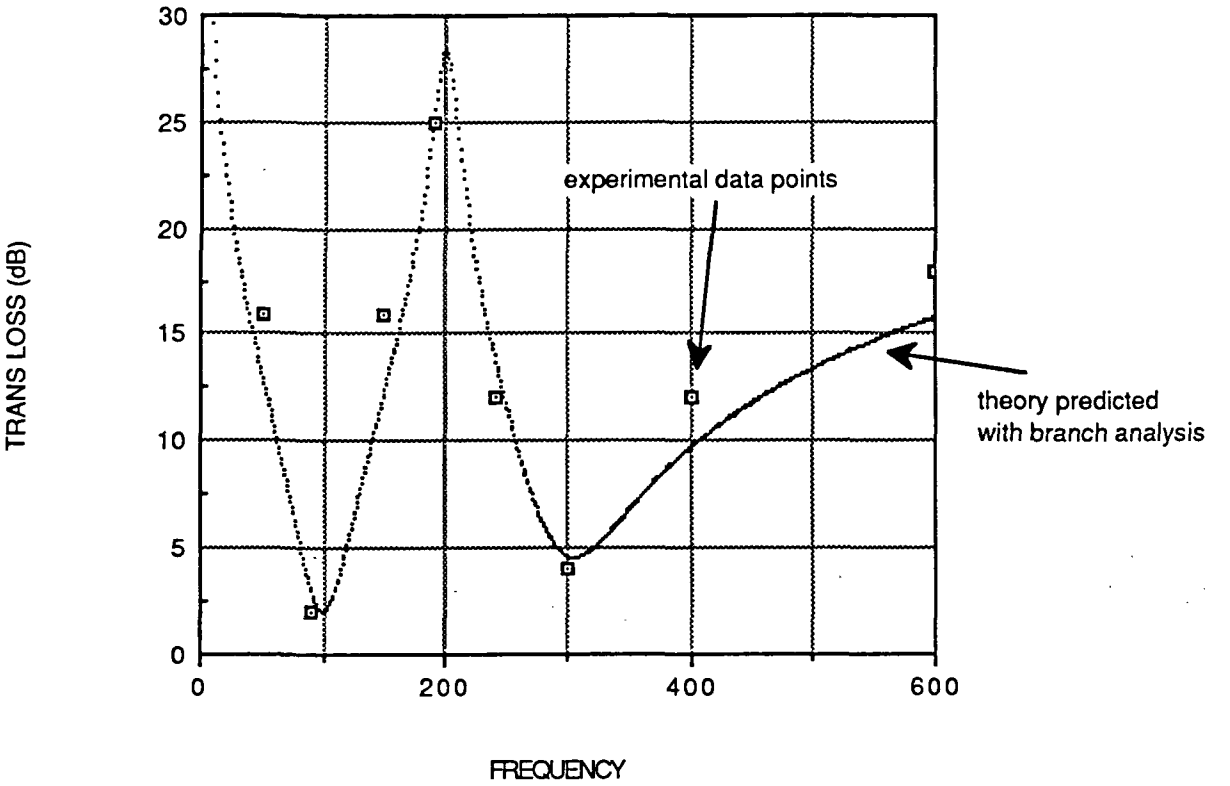

Figure 2c-1: Branch analysis theory plotted against single ART panel experimental data.

Section 2d. Analysis of the ART Concept Using Real Panels

In all previous ART development, the aircraft panels have been modelled as simple spring-mass-damper systems. Preliminary work has been completed on a method which will allow analysis of the ART concept using real panel sections. In practice, an aircraft is composed of an outer skin attached to a series of ribs and stringers. This panel edge boundary condition is truly not pinned or clamped; however, the method being developed can be considered for either of these boundary conditions. In order to investigate the possibility of solving any such system, a model problem of reduced complexity is considered. The geometry for this solution method is shown in Figure 2d-1. Any results obtained for this reduced model problem can be verified with existing analysis; hence, it is a good test problem for development and debugging of the full plate solution.

Figure 2d-1 considers a two dimensional solution to the plate equation with an acoustic input. The panels are of width W and have pinned boundary conditions. A reflecting

impedance Z_b is contained a distance L from the panel array. Other notation conventions are noted in Figure 2d-1.

The method of choice involves a combination of standard solutions to the two dimensional wave equation

$$\frac{\partial^2 p}{\partial t^2} + \frac{\partial^2 p}{\partial y^2} - \frac{1}{c^2}\frac{\partial^2 p}{\partial t^2} = 0 \qquad 2d.1$$

with the associated acoustic boundary conditions

$$\frac{\partial p}{\partial y}(x,-\frac{W}{2},t) = \frac{\partial p}{\partial y}(x,\frac{W}{2},t) = 0 \qquad 2d.2$$

coupled with a Galerkin solution for the two dimensional plate equation

$$-D_E \frac{\partial^4 w}{\partial y^4} + p - \rho\frac{\partial^2 w}{\partial t^2} = Q_t(w) \qquad 2d.3$$

For each panel to be considered, a general set of trial solutions is then assumed for the Galerkin method. These trial solutions are of the form

$$w_j(y,t) = \sum_{k=1}^{K} A_k^j e^{i\omega t} \sin(\frac{k\pi y}{W}) \qquad 2d.4$$

Here j equals the number of panels to be considered (two for the model problem) and k is the number of modes in the Galerkin trial solution. To simplify the algebra for this demonstration problem, only a one mode solution is presented here.

Separate acoustic solutions may be written for $x < 0$ and for $x > 0$. For $x < 0$ or the external portion of the fuselage, the acoustic pressure may be expressed as

$$\begin{aligned} P_{EX}(x,y,t) = {} & \hat{P}_0^I e^{i(\omega t - kx)} + \hat{P}_0^R e^{i(\omega t + kx)} \\ & + \sum_{m=1}^{\infty} \hat{P}_m^R e^{i\omega t} e^{\hat{k}_x} \cos(\frac{2m\pi}{W})y \\ & + \sum_{m=1}^{\infty} \tilde{P}_m^R e^{i\omega t} e^{\tilde{k}_x} \sin(\frac{[2m-1]\pi}{W})y \end{aligned} \qquad 2d.5$$

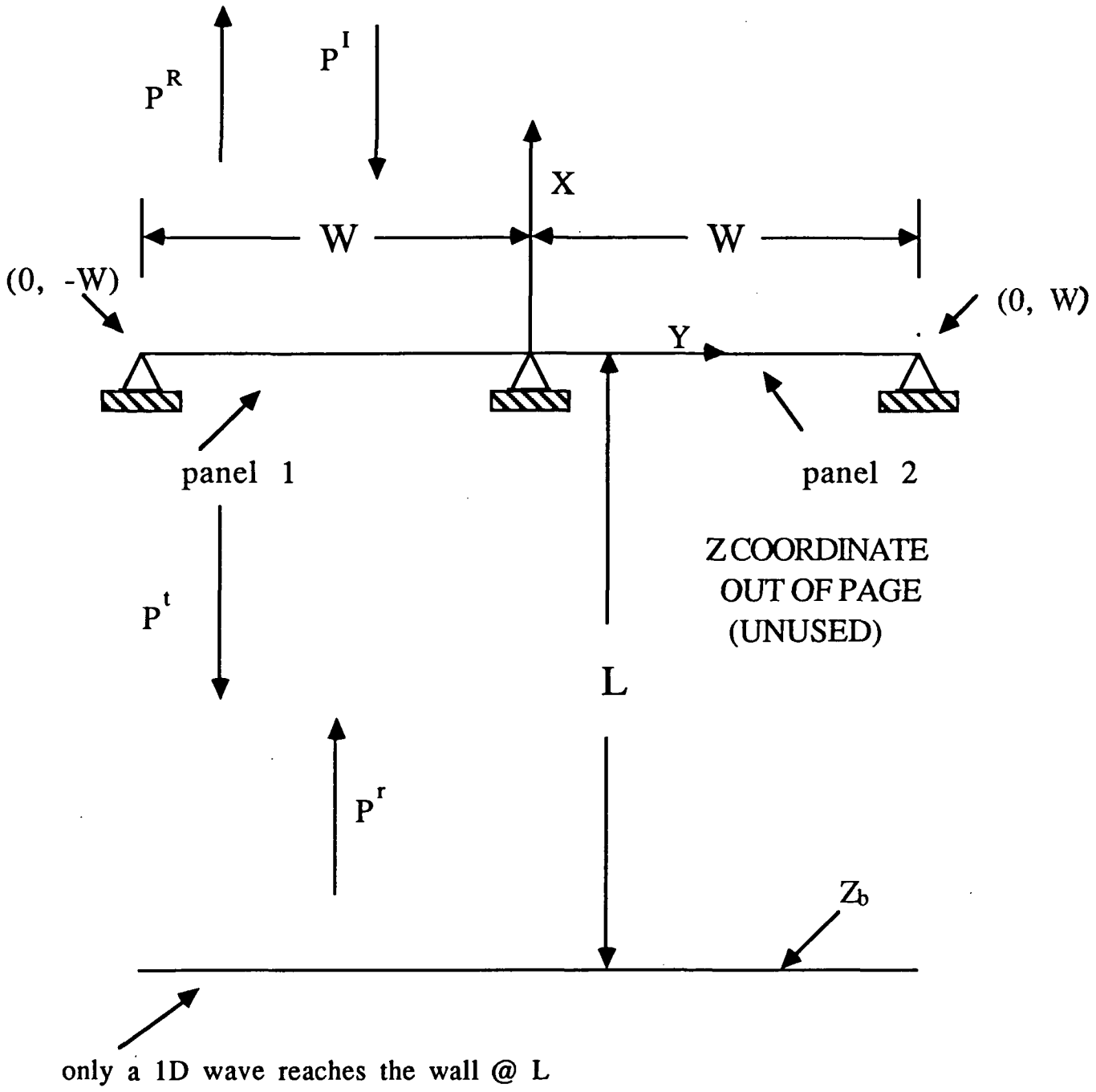

NOTATION:

Capital superscripts indicate waves outside fuselage
Small superscripts indicate waves inside fuselage

Panels are infinitely deep into the page

Figure 2d-1: Model Problem for Plate Solution Development

A similar general solution may be written for x > 0, or on the aircraft interior, as

$$P_{IN}(x,y,t) = \hat{P}_0^t e^{i(\omega t - kx)} + \hat{P}_0^r e^{i(\omega t + kx)} + \sum_{m=1}^{\infty} \hat{P}_m^t e^{i\omega t} e^{-\hat{k}_x} \cos(\frac{2m\pi}{W})y + \sum_{m=1}^{\infty} \tilde{P}_m^t e^{i\omega t} e^{-\tilde{k}_x} \sin(\frac{[2m-1]\pi}{W})y \qquad 2d.6$$

where

$$\hat{k}_x = \sqrt{\frac{\omega^2}{c^2} - (\frac{2m\pi}{W})^2} \qquad 2d.7$$

and

$$\tilde{k}_x = \sqrt{\frac{\omega^2}{c^2} - (\frac{[2m-1]\pi}{W})^2} \qquad 2d.8$$

The associated cutoff condition for this system supposes that

$$\omega < \sqrt{c^2 (\frac{[2m-1]\pi}{W})^2} \qquad 2d.9$$

and

$$\omega < \sqrt{c^2 (\frac{2m\pi}{W})^2} \qquad 2d.10$$

From elementary acoustic impedance relationships, we may write a relationship between the reflected and transmitted waves at the downstream impedance Z_b as

$$\frac{\hat{P}_0^r}{\hat{P}_0^t} = e^{-i2kL} \frac{(\frac{Z_b}{\rho_0 c} - 1)}{(\frac{Z_b}{\rho_0 c} + 1)} \qquad 2d.11$$

Differentiation of the trial solution for the panel deflections yields the panel velocities. We wish to determine the unknown Galerkin coefficients in the trial solution. With the previous

expressions for the upstream and downstream pressures, a relationship can be established for the determination of the unknown Galerkin expansion coefficients using the momentum equation

$$\frac{\partial u}{\partial t} = -\frac{1}{\rho_0}\frac{\partial p}{\partial x} \qquad 2d.12$$

and the plate boundary conditions of

$$u(x=0-) = u(x=0+) = i\omega A_k^j e^{(i\omega t)} \sin(\frac{\pi}{W})y \qquad 2d.13$$

Next orthogonality is applied to the general pressure expressions to determine the values of the unknown amplitudes P^r,P^t,P^R, and P^I. Additionally, the acoustic boundary conditions are applied. The summary of these actions is shown below.

$$\hat{P}_0^I - \hat{P}_0^R = \rho_o c(\frac{-i\omega A_1^1 + i\omega A_1^2}{\pi}) = \hat{P}_0^t - \hat{P}_0^r \qquad 2d.14a$$

$$\hat{P}_m^t = \hat{P}_m^R = 0 \qquad 2d.14b$$

$$\tilde{P}_m^t = \frac{-\omega(A_1^1 + A_1^2)\rho_0 c}{2\tilde{k_x}} \qquad 2d.14c$$

$$\tilde{P}_m^R = \frac{\omega(A_1^1 + A_1^2)\rho_0 c}{2\tilde{k_x}} \qquad 2d.14d$$

Now turning to the structural portion of the solution, a pressure differential across the plate may be calculated as the sum of the pressures on all sides of the plate, given by

$$\Delta p = P^I + P^R - (P^t + P^r) \qquad 2d.15$$

Thus the pressure differential for the plate equation reduces to

$$\Delta p = 2P^I - 2P^t + \rho_0 c\omega\left[\sum_{m=1}^{\infty} \sin(\frac{[2m-1]\pi}{W})y\left[\frac{(A_1^1 + A_1^2)}{\tilde{k}_x}\right]\right] \qquad 2d.16$$

By Galerkin's method, a variation in the trial solution is defined as

$$\delta\Phi_j(y) = \delta A_k^j e^{i\omega t} \sin\frac{k\pi y}{W} \qquad 2d.17$$

and j ordinary differential equations with k modes are created from

$$\int_0^w Q_i(w)\,\delta\Phi_i(y)dy = 0 \qquad 2d.18$$

Thus an acoustic solution is coupled to a structural partial differential equation governing the plate behavior; furthermore, this partial differential equation is restated as j ordinary differential equations which can be integrated to produce j equations. These j equations can be solved exactly analytically if the number of modes in the Galerkin solution is small; otherwise, the algebra can be cumbersome. Alternately, (j+1) equations may be solved numerically for the A_k^j coefficients in the trial solution, where the additional equation is a continuity equation obtained earlier from application of the various boundary conditions. For the current case of two panels with a one mode Galerkin trial solution, the three equations obtained are shown below.

$$-A_1^1\frac{\pi^4}{2W^3}+\frac{\rho}{D_E}\omega^2 A_1^1\frac{W}{2}-\frac{4}{D_E}\hat{P}_0^t=\frac{4}{D_E}\hat{P}_0^I$$

$$-A_1^2\frac{\pi^4}{2W^3}-\frac{\rho}{D_E}\omega^2 A_1^2\frac{W}{2}+\frac{4}{D_E}\hat{P}_0^t=\frac{-4}{D_E}\hat{P}_0^I \qquad 2d.19$$

$$\frac{-i\omega A_1^1}{\pi}+\frac{i\omega A_1^2}{\pi}-\frac{\hat{P}_0^t}{\rho_0 c}\left(1-e^{-i2kL}\frac{\left(\frac{Z_b}{\rho_0 c}-1\right)}{\left(\frac{Z_b}{\rho_0 c}+1\right)}\right)=0$$

This represents a system of three equations and three unknowns which may be solved numerically or analytically. A more general model with a full, three dimensional acoustic solution to a four panel clamped geometry, with three or more modes in the Galerkin trial solution would have to be solved numerically.

SECTION 3. EXPERIMENTAL WORK

Section 3a. Incorporation of the New Data Acquisition System

Two new methods for data taking are currently being developed in the laboratory, and each is designed to interface with the Macintosh II computer. The first method uses a combination of the analog-to-digital capability of the Macintosh II computer, coupled with the software processing capability of the LabVIEW software. White noise is used to drive the sound source in the ART duct experiment, and microphone signals are monitored via the A/D connection. LabVIEW is then used to spectrum analyze the data obtained for each microphone, and differencing of the signals may be done using LabVIEW, simple FORTRAN programming, or using available software in the graphics package on the Macintosh II. The second method, shown below, uses a Bruel and Kjaer pure tone generator (driven mechanically through the frequency range of interest and tracked with simple electronic means) to power the sound source. The AC electrical microphone signals are then converted to a DC signal which is proportional to the sound pressure level of the signal. Three converter channels have been constructed and calibrated along with a frequency tracking device. Work is proceeding on appropriate A/D software which will complete operation of the system. Thus, the laboratory will have two separate methods of obtaining data for the ART experiments.

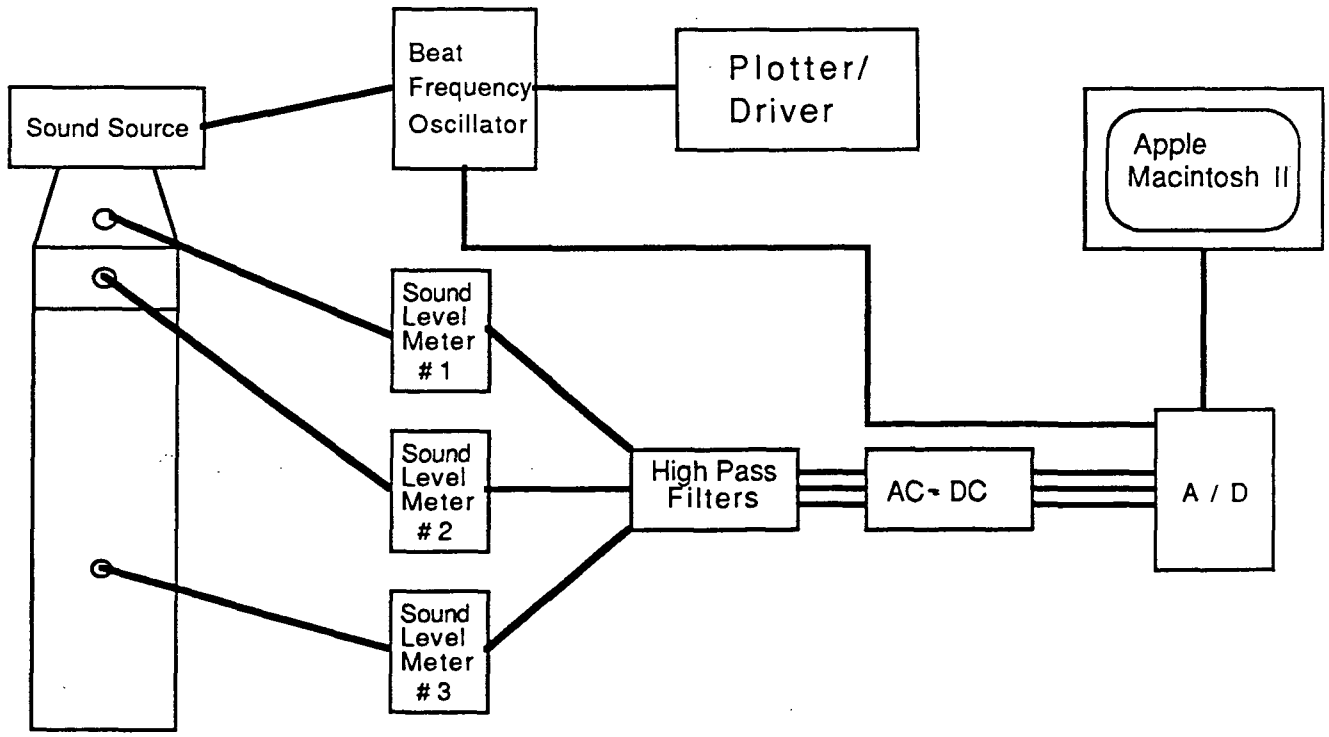

Figure 3a-1: Data acquisition setup.

Section 3b. Two Dimensional Art Experiment Development

Preparation has begun on the two-dimensional experiment in which the effects of the aircraft's propellers on the ART panels will be explored. This section describes a method to simulate a propeller passage through the use of a phase controlled loudspeaker array. The technique employs a line of speakers transmitting identical pure tones which are consecutively out of phase. The pressure field created moves down the array, as shown in Figure 3b-1, representing a propeller blade passing. The system and circuitry to perform this task are detailed. In addition, a control system is presented which allows for automated operation.

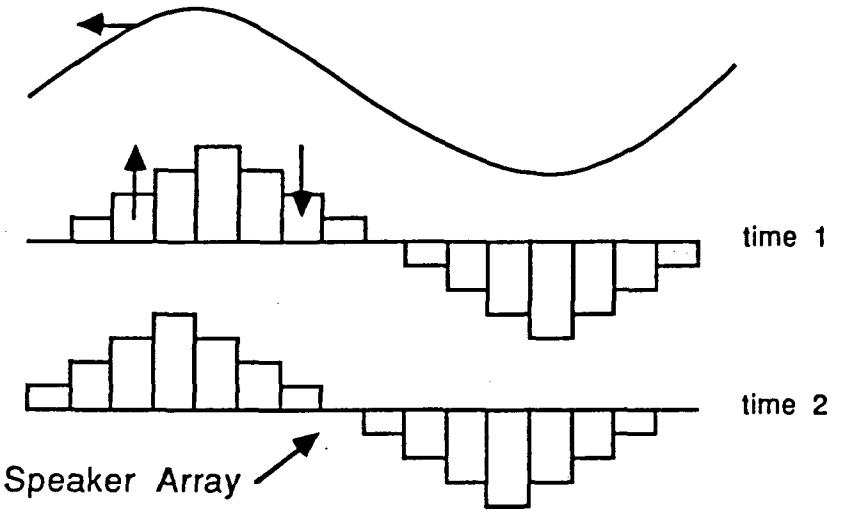

Figure 3b-1: Desired motion of an external pressure field to model aircraft propeller passage.

Loudspeaker Array

The loudspeaker array system will consist of a signal source, phase shifting circuits, amplifiers, and loudspeakers as shown in Figure 3b-2. Under normal operation all phase shifters would add the same shift to the signal. For instance if the phase shift were 10 degrees, the second speaker would be out of phase by that amount from the first. Similarly, the third speaker would be 10 degrees out from the second and so on. The signals would be amplified as shown between the shifters and speakers allowing for individual volume control.

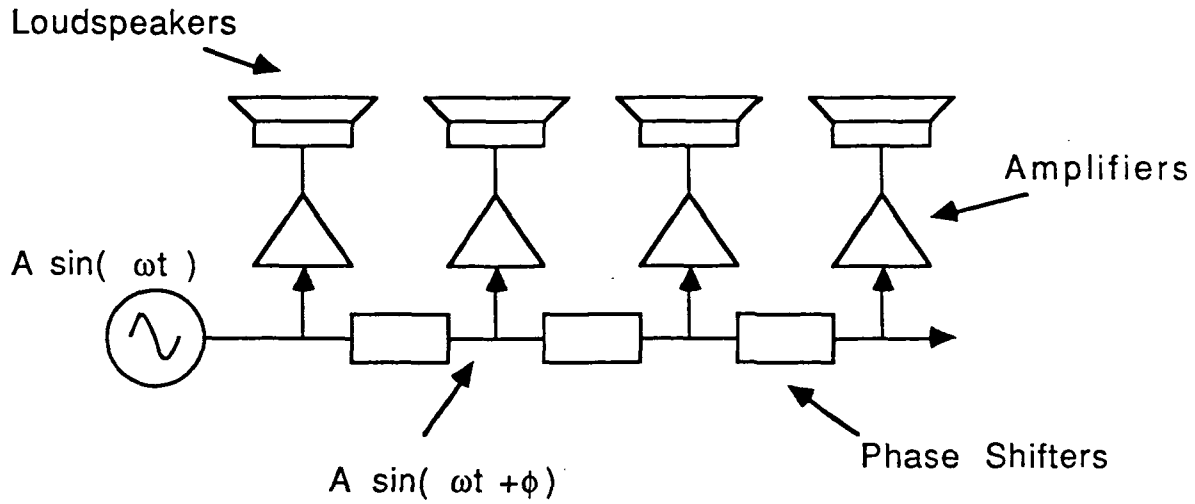

Figure 3b-2: Overall schematic of circuitry to simulate propeller pressure field.

Phase Angle

The phase angle between the speakers depends on the speaker spacing, the excitation frequency and the desired wave speed, and may be expressed as

$$\phi = \frac{l \times 360 \times f}{n \times c_p}$$

where

$\phi \equiv$ phase angle (degrees)
$l \equiv$ length of speaker array (ft)
$f \equiv$ frequency (Hz)
$c_p \equiv$ wave speed (ft / sec)

Small phase shifts (less than 90 degrees) realistically simulate the propeller pressure field; however larger ones do not. The relationship therefore has some limitations. In addition, the physical dimensions of available speakers must be taken into account. A reasonable speaker spacing of eight inch centers or nine speakers for a six foot array is obtainable. The above expression would then limit the wavenumber to a maximum value of 2.36. The minimum allowable wave speed (ft / sec) would therefore be 2.66 times the frequency (Hz).

Phase Shifter

A simple phase shifter curcuit can be constructed using an operational amplifier with several external resistors and a capacitor as shown in Figure 3b-3.

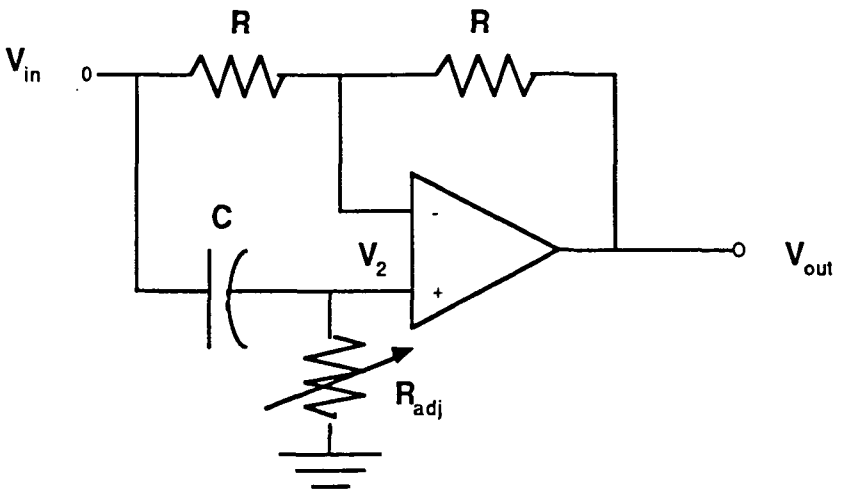

Figure 3b-3: Phase shifting schematic for propeller simulation circuitry.

This circuit can be analyzed by equating the current flow in the branches. First, the current through the two resistors gives

$$\frac{V_{in} - V_2}{R} = \frac{V_2 - V_{out}}{R}$$

and the current thourgh the capacitor branch yields

$$\frac{V_{in} - V_2}{1/j\omega C} = \frac{V_2}{R_{adj}} .$$

Combining the above equations gives

$$V_{out} = \frac{(-1 + j\omega CR_{adj})}{(1 + j\omega CR_{adj})} V_{in}$$

When simplified the transfer function yields

$$\frac{(\omega CR_{adj})^2 - 1}{(\omega CR_{adj})^2 + 1} + j\frac{2\omega CR_{adj}}{(\omega CR_{adj})^2 + 1}$$

which can be shown to have a unity gain with a phase angle of

$$\phi = \mathrm{Tan}^{-1}\frac{2\omega CR_{adj}}{(\omega CR_{adj})^2 - 1}$$

Additional transformation produces

$$\phi = 180 - 2\mathrm{Tan}^{-1}\omega CR_{adj}.$$

This expression for the phase shift depends on the signal frequency, the capacitance, and adjustable resistance. The characteristics of the operational amplifier and the feedback resistors are not contributing factors. By equating the above expression to the required physical phase angle expression, the relationship between the resistance and frequency for constant wave speeds is shown in Figure 3b-4.

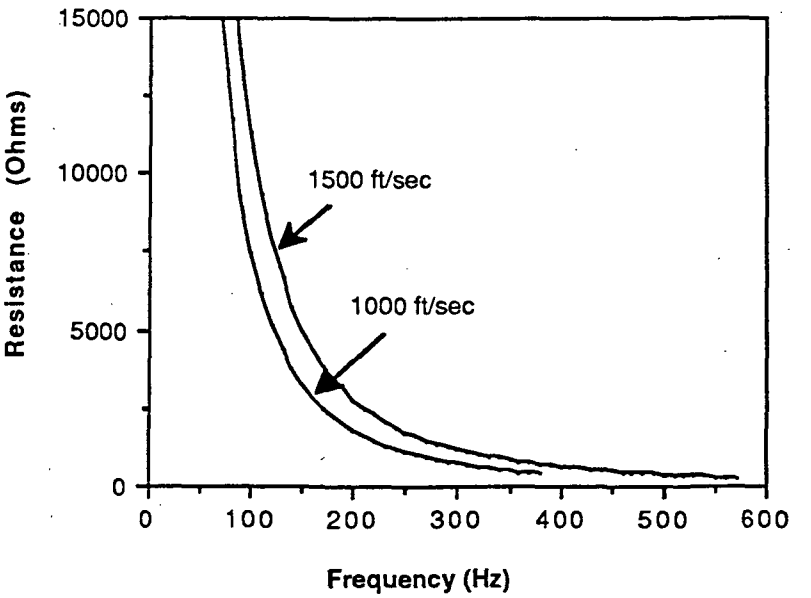

Figure 3b-4: Relationship between the resistance and frequency for constant wave speeds (9 speakers, C = 1.0 μf).

Voltage Controlled Resistor

Simple operation of the phase shifters can be accomplished through the adjustment of the potentiometers; however, the manual turning of pots for large speaker arrays is restrictive and precludes automated operation. A solution to this problem is to use Voltage Controlled Resistors (VCRs) to control the phase shifts. A VCR can be realized through the use of a Field Effect Transistor (FET). As shown in Figure 3b-5, the FET's ohmic region characteristics are such that the drain-to-source resistance can be controlled by the gate-to-source voltage. The relationship between the drain-to-source resistance and the gate-to-source voltage is, however, nonlinear and FET dependent.

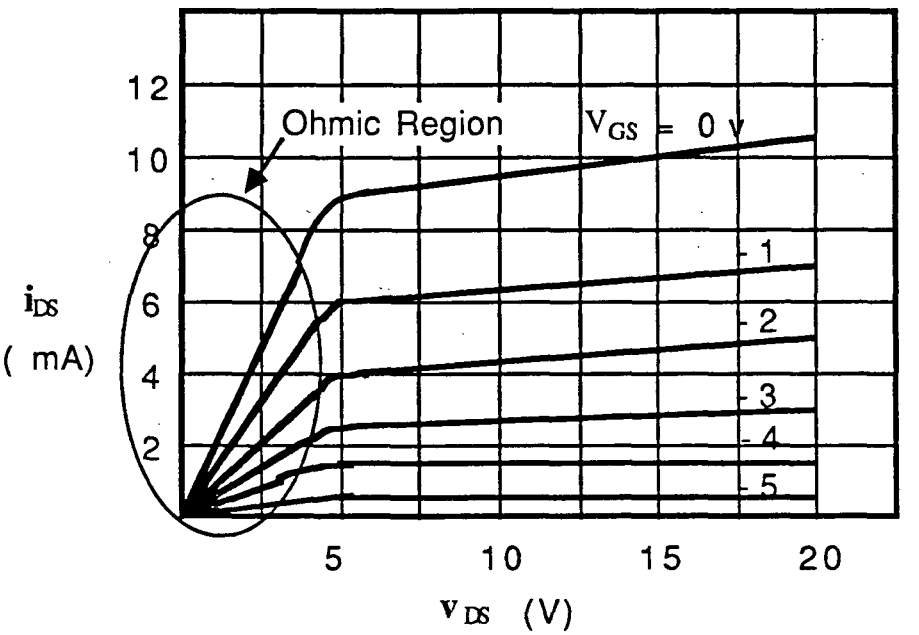

Figure 3b-5: Typical FET Characteristics.

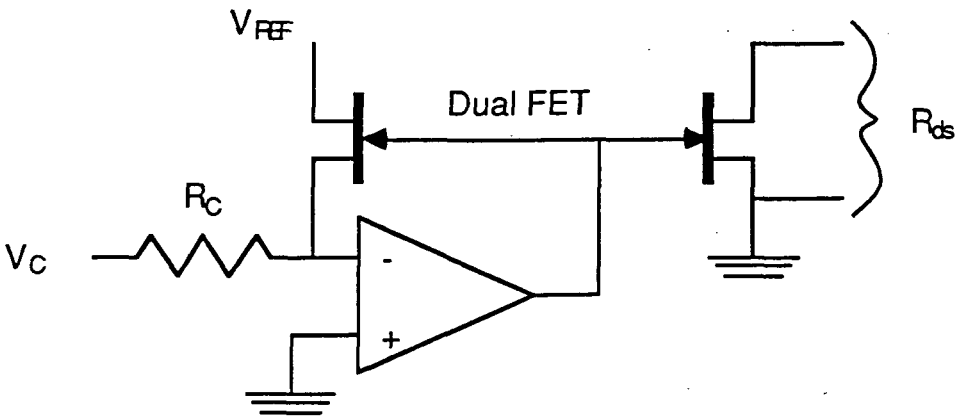

Figure 3b-6: Linear VCR circuit with dual FET and amplifier.

A repeatable linear VCR circuit can be constructed with a dual FET and an op amp as shown in Figure 3b-6. The negative control voltage ' V_C ' causes current to flow from the inverting input of the op amp through the control resistor ' R_C '. Circuit analysis shows that this current is supplied by the FET from the reference voltage ' V_{ref} '. The op amp's output delivers the necessary voltage to the FET's gate. The free half of the FET sees the same gate-to-source voltage and can be used as a VCR with the following property:

$$R_{ds} = |V_{REF}| R_C / |V_C| .$$

A calibration curve comparing one such VCR to the above expression is presented below.

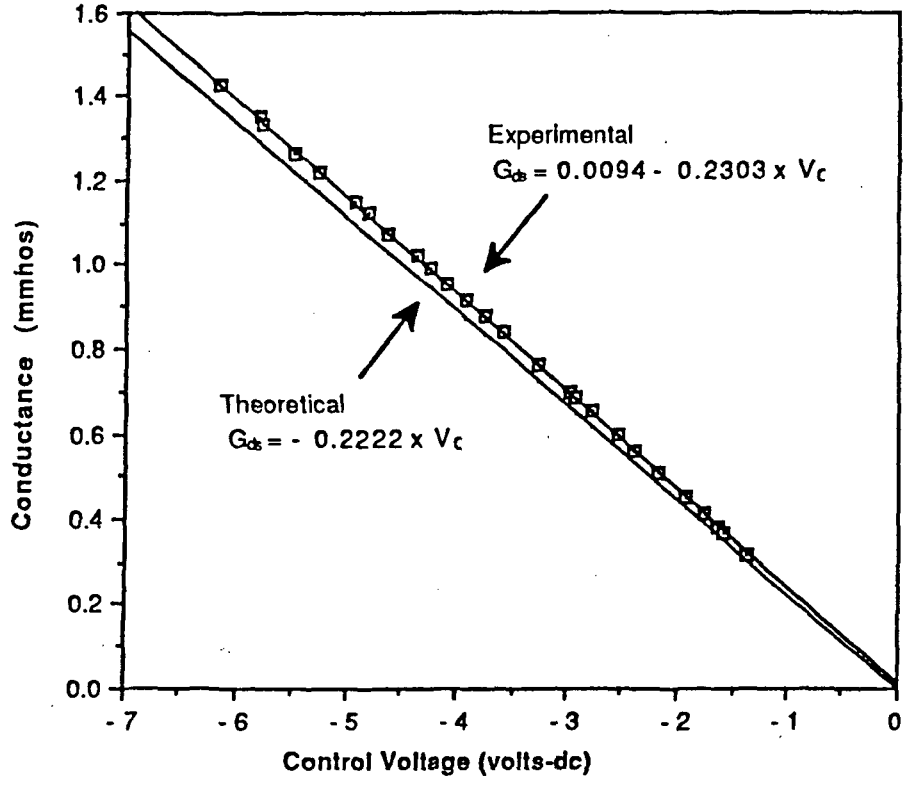

Figure 3b-7: Typical calibration curve for the VCR.
(V_{REF} = 0.045 v, R_C = 100 kΩ)

Automated Control

The entire system of phase shifters can be automated so that the phase shifts can be adjusted by a single controller. The Macintosh II computer with digital-to-analog and analog-to-digital capabilities can supply the necessary voltage to the VCRs in the phase shift circuits depending on other desired parameters. An example of an automated system is shown below.

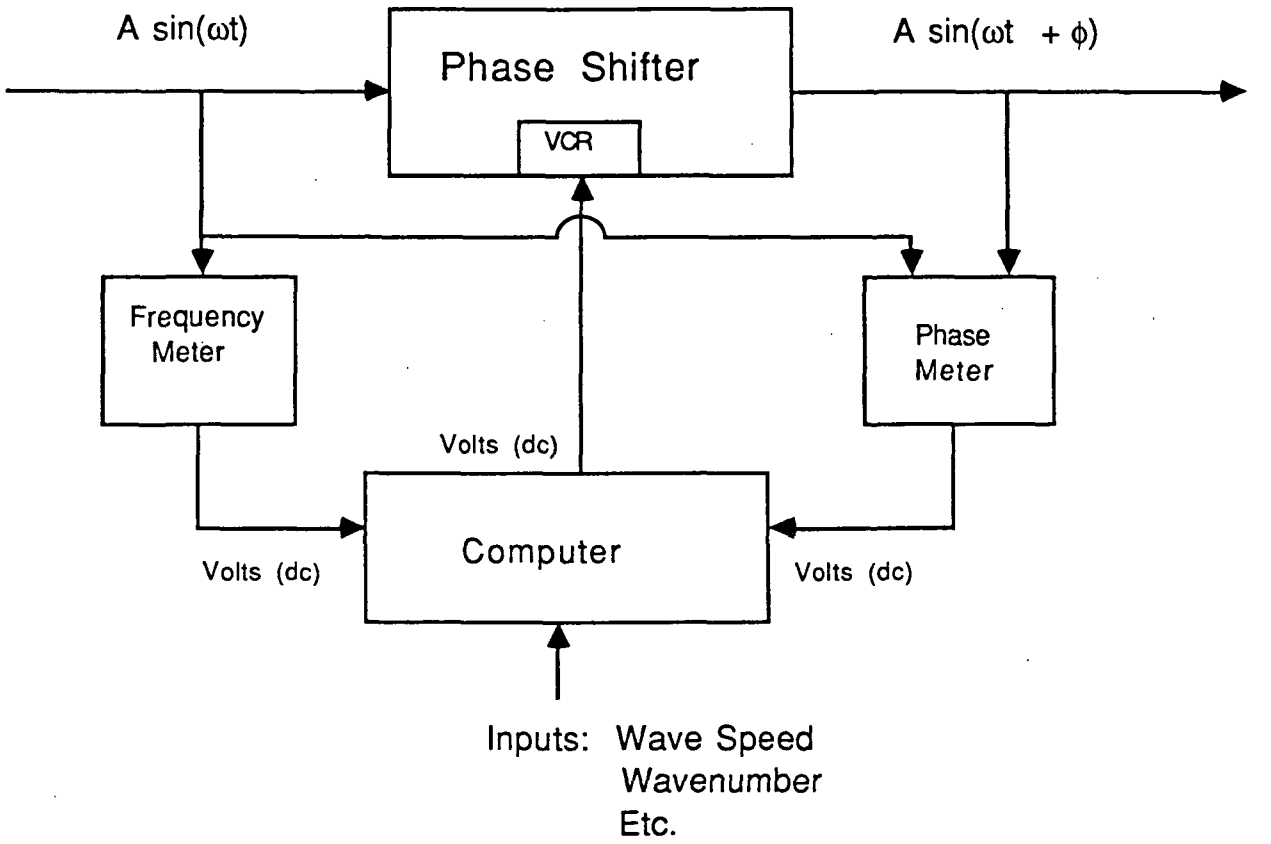

Figure 3b-8: Schematic for automatic control of propeller simulation circuitry.

A frequency-to-dc meter provides the computer with the signal frequency. Parameters such as the wave speed and wavenumber are manually inputed to the computer in order to control the phase shifts. The use of a phase-to-dc meter can be added as a feedback loop to make the system self-compensating. Only one of these setups is required since the same voltage can be sent to all of the VCRs in the system.

Frequency Meter

A frequency-to-dc meter can be contructed with several op amps and comparators along with some external resistors and capactitors. The circuit is shown below.

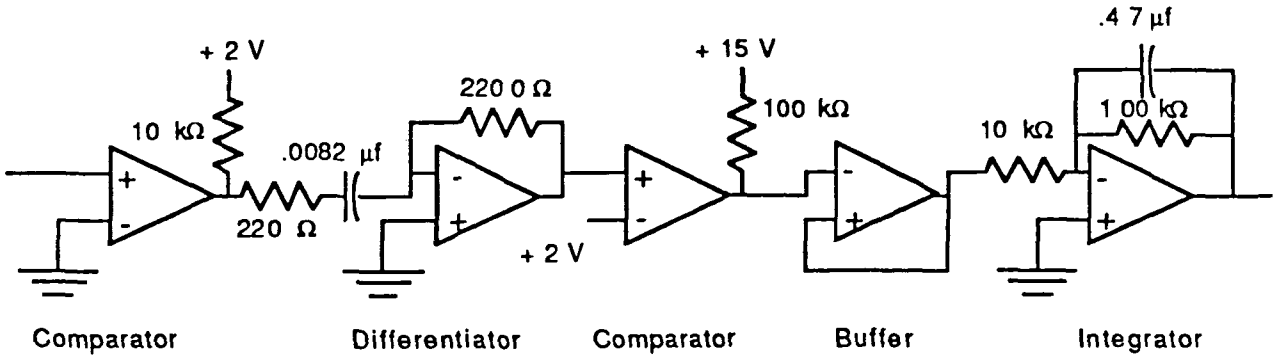

Figure 3b-9: Frequency to DC meter for monitoring purposes.

The comparator creates a rectified square wave with a peak voltage of 2 volts. The differentiator then transforms the squarewave into one pulse per cycle. A second pass through a comparator makes the pulses uniform with a width which is small compared to the the frequency range in question. Finally, an integrator time averages these pulses giving a dc voltage. This output can then be used in the control system. A typical calibration plot for the meter is shown in Figure 3b-10.

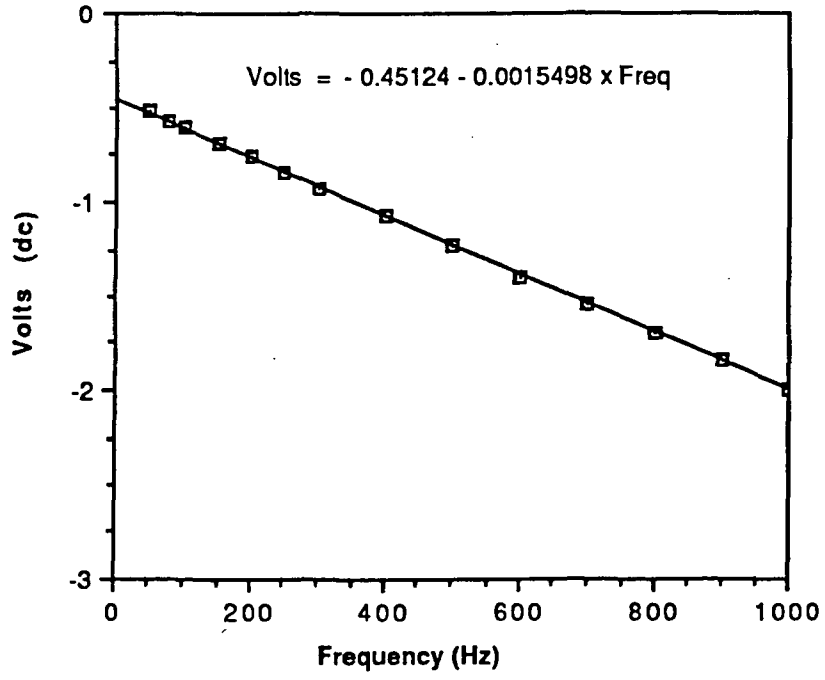

Figure 3b-10: Typical calibration plot for the frequency meter.

Phase Meter

The phase-to-dc meter schematic shown in Figure 3b-11 has a concept similar to the frequency meter however digital TTl logic is employed.

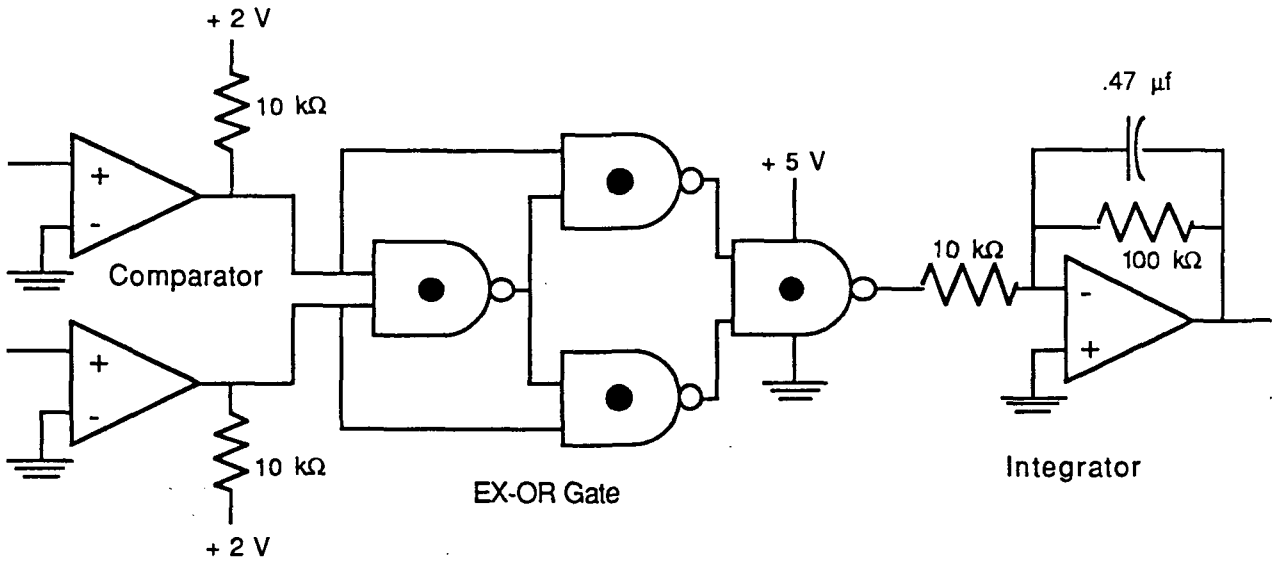

Figure 3b-11: Phase-to-dc meter schematic.

The comparators transform the sine wave inputs into rectified square waves with amplitudes of 2 volts. The signals are then fed into an exclusive OR gate constructed from four NAND gates. The output from this device is high when one or the other of the inputs is high as indicated by the diagram below.

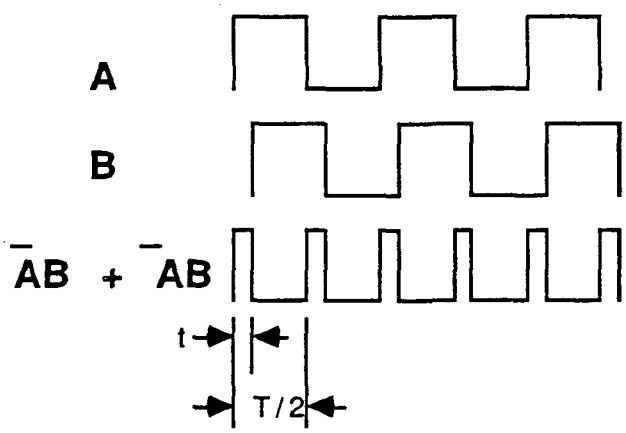

Figure 3b-12: Logic diagram for Ex-OR gate.

The time of the high signal 't' is proportional to the phase angle between the signals as follows:

$$\phi = \frac{180 \times t}{T/2}$$

When t=0, the phase angle equals zero; similarly, when t = T /2, the phase angle equals 180. The integrator time averages the pulses resulting in a DC voltage proportional to the phase shift. A typical calibration curve is presented in Figure 3b-13.

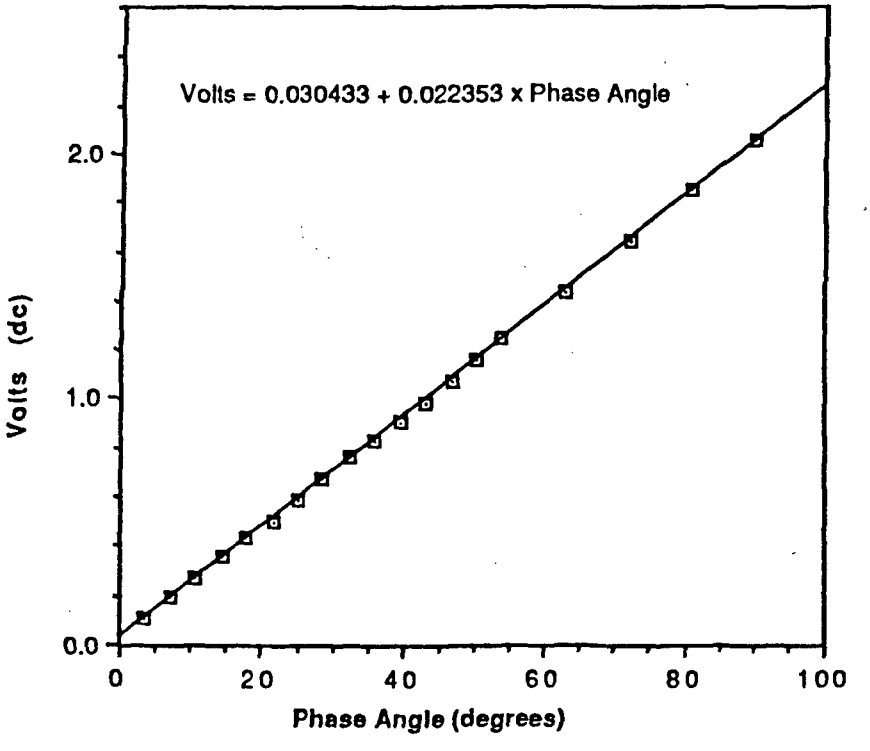

Figure 3b-13: Phase meter calibration curve.

Section 3c.Double Panel Duct Experiments

The Dual Panel Wall experiments (DPW) are designed to explore the effect of a second wall on the performance of the Alternate Resonance Tuning concept. In this manner, it is possible to mimic the inner skin/outer skin construction of an airplane fuselage. As shown in Figure 3c-1, four panels are used in two walls of two panels each, placed in a duct which is effectively one-dimensional. One of the two-panel walls is placed near the sound source (upstream) with a coupling spacer to the downstream panel. Transmission loss data is then taken by placing one microphone just upstream of the first wall, a second microphone in the coupling duct, and a

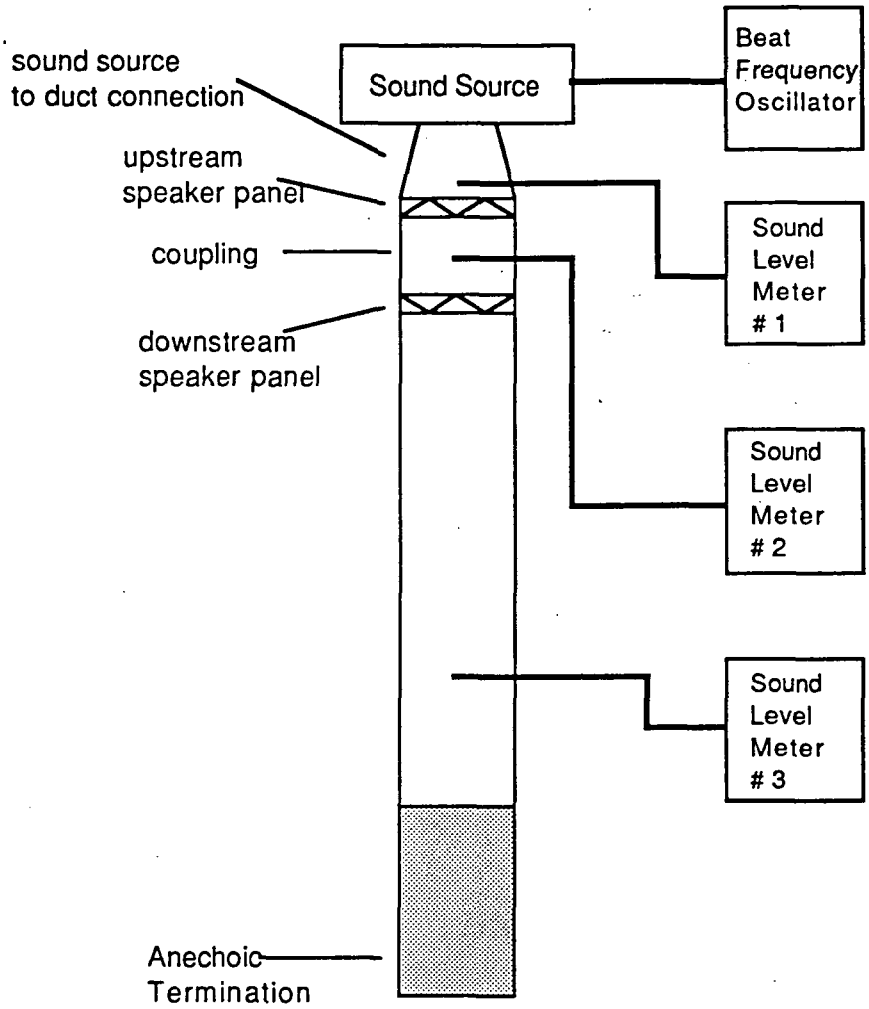

Figure 3c-1: Dual panel wall experimental apparatus showing the sound source, coupling between the upstream and downstream speaker panels, and microphone layout.

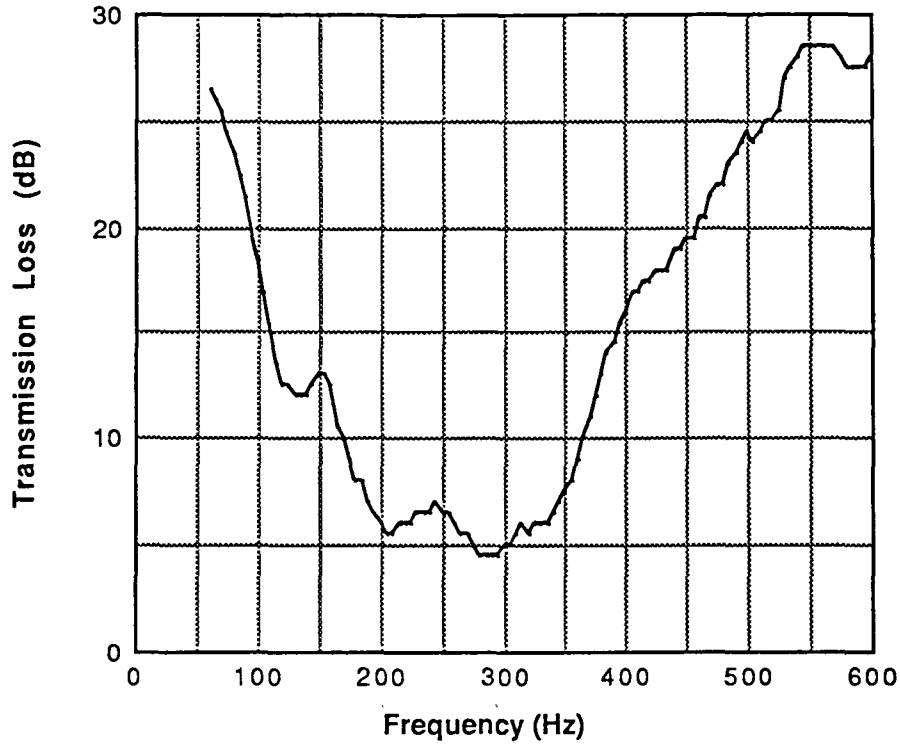

Figure 3c-2: Transmission loss data for the dual panel wall experiment with four identical speakers and the 7" coupling.

third microphone downstream of the wall setup. The termination impedance is anechoic. This apparatus allows for acquistion of transmission loss data across each individual wall, and across both walls simultaneously.

Initially, four identical panels with resonant frequencies at 200 Hz were placed in the duct, and transmission loss data for this case is shown in Figure 3c-2 above. Previous data has shown the transmission loss reaches a minimum at 200 Hz, where the loss is only 6 dB. However, there is another point of minimum transmission loss at approximately 300 Hz. This "coupling resonance" arises due to the dynamics of panels and the coupling duct air spring. At the first minimum, the four panels move in phase with each other, but at the second minimum, the two walls of panels move out of phase with each other. This phenomena can be seen in the plot of the panel phase shifts for this setup (Figure 3c-3).

The next step was to replace the downstream identical panels with ART panels, representing the possible placement of ART panels on an interior airplane wall. The ART panels have resonant frequencies near 100 and 300 Hz. Figure 3c-4 shows the transmission loss data

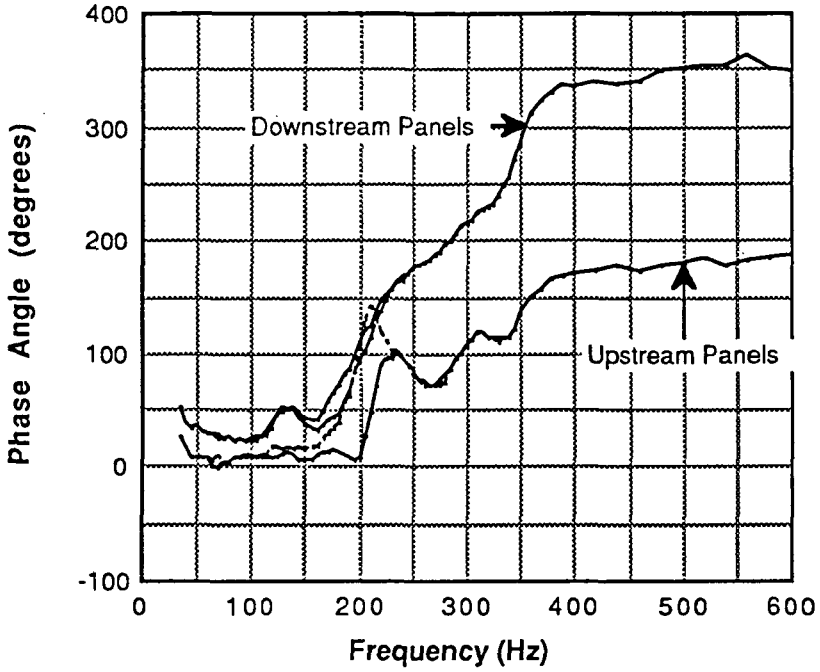

Figure 3c-3: Phase angle data for the dual panel wall experiment with four identical speakers and 7" coupling.

for this setup. As expected, there are two minima: one near 100 Hz and one near 300 Hz. However, at the design frequency of 200 Hz, a transmission loss of 24 decibels was achieved, showing that the ART concept functions well in a two-wall environment. The coupling resonance first noted in the previous setup can also be seen as a local minimum in the transmission loss occurring at 350 Hz. On the plot of the panel phase shifts for this case (Figure 3c-5), the ART panels achieve nearly out-of-phase motion between 150 and 250 Hz.

The next step was to replace the downstream identical panels with ART panels, representing the possible placement of ART panels on an interior airplane wall. The ART panels have resonant frequencies near 100 and 300 Hz. Figure 3c-4 shows the transmission loss data for this setup. As expected, there are two minima: one near 100 Hz and one near 300 Hz. However, at the design frequency of 200 Hz, a transmission loss of 24 decibels was achieved, showing that the ART concept functions well in a two-wall environment. The coupling resonance first noted in the previous setup can also be seen as a local minimum in the transmission loss occurring at 350 Hz. On the plot of the panel phase shifts for this case (Figure 3c-5), the ART panels achieve nearly out-of-phase motion between 150 and 250 Hz.

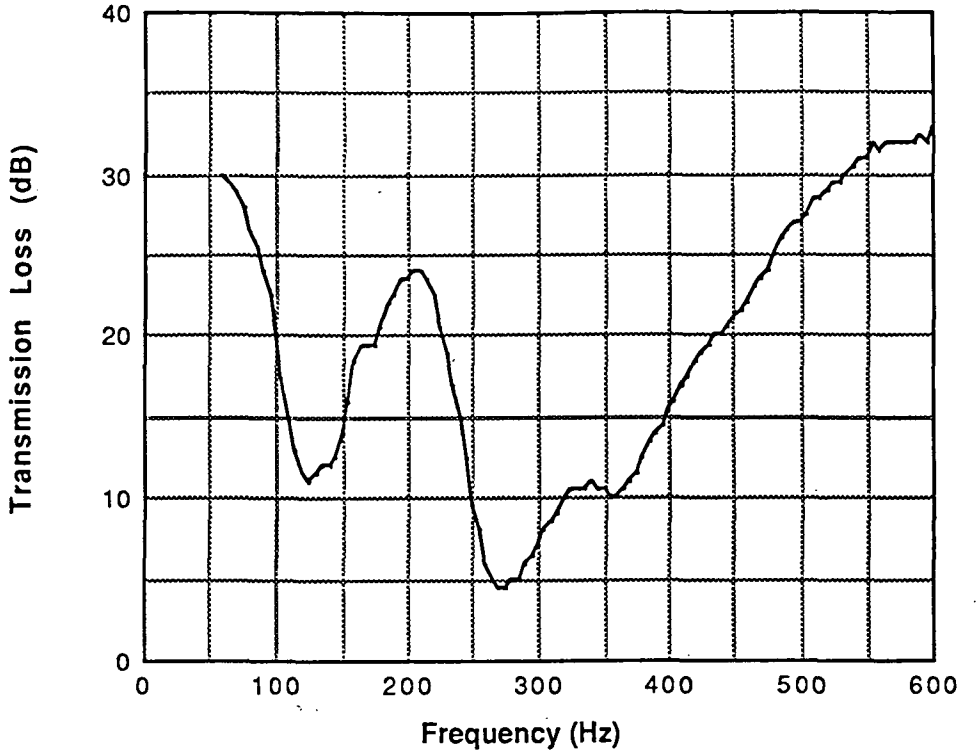

Figure 3c-4: Transmission loss data for the dual panel wall experiment with identical speakers upstream and ART speakers downstream with the 7" coupling. Speaker resonances are approximately 100 and 300 Hz.

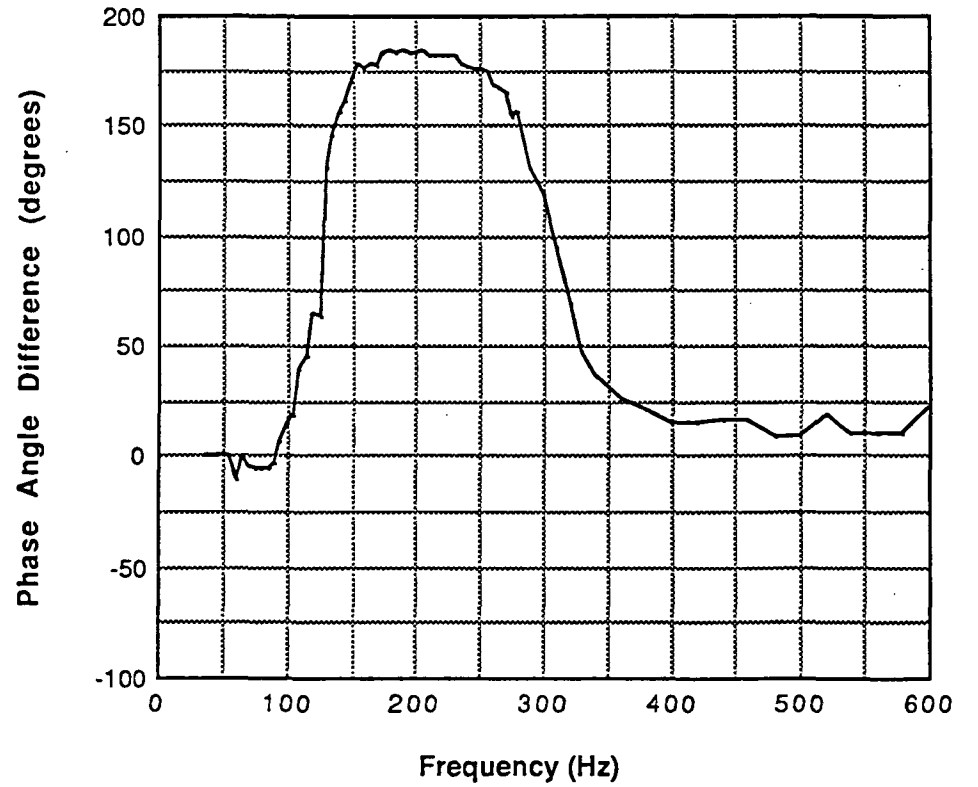

Figure 3c-5: Phase difference between ART downstream speakers for dual panel wall experiment with two identical speakers upstream and two ART speakers downstream and the 7" coupling.

Knowing that the ART concept functions in a two-wall environment, it was desired to see how changing the size of the coupling would affect the above results. Two different couplings were then built, one with a separation of two inches and one with a separation of one inch, and the above data was retaken. Note that the passive speakers used as panels have a diameter of approximately four inches. Figure 3c-6 shows the transmission loss results for the two inch coupler and four identical panels. Again, the minimum occurs at 200 Hz, the resonance of the panels. However, the coupling resonance minimum has shifted and occurs as a broad minimum around 500 Hz. This shift in the coupling resonance can be attributed to the stiffening of the air spring as its size is reduced. Figure 3c-7 shows the same configuration with the one inch coupler. The results are approximately the same, except that the coupling resonance has again shifted, occurring between 550 and 600 Hz.

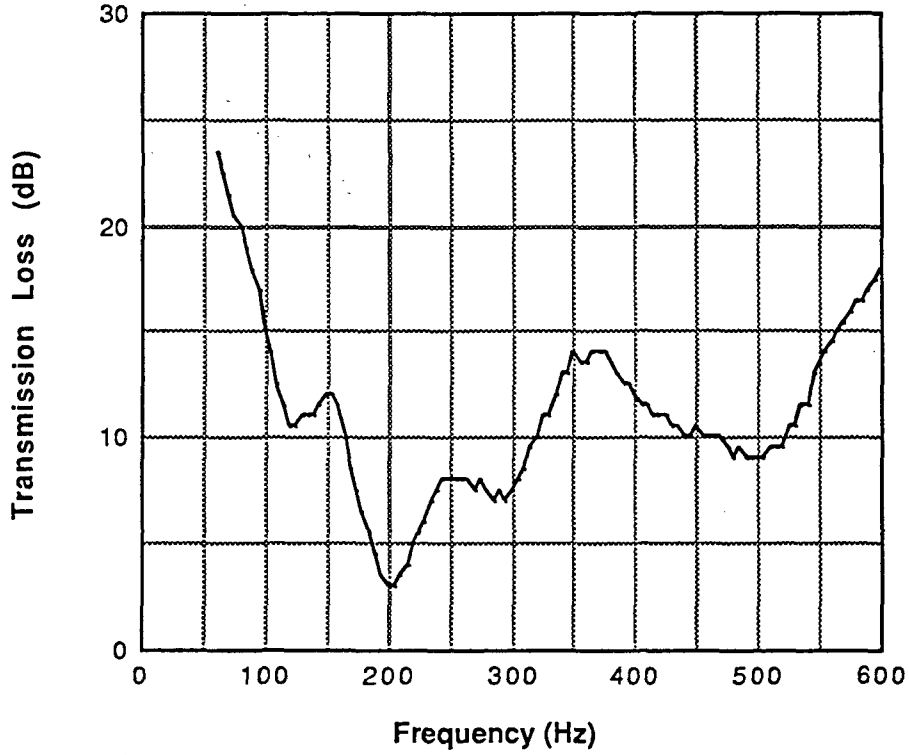

Figure 3c-6: Transmission loss data for the dual panel wall experiment with four identical speakers and the 2" coupling.

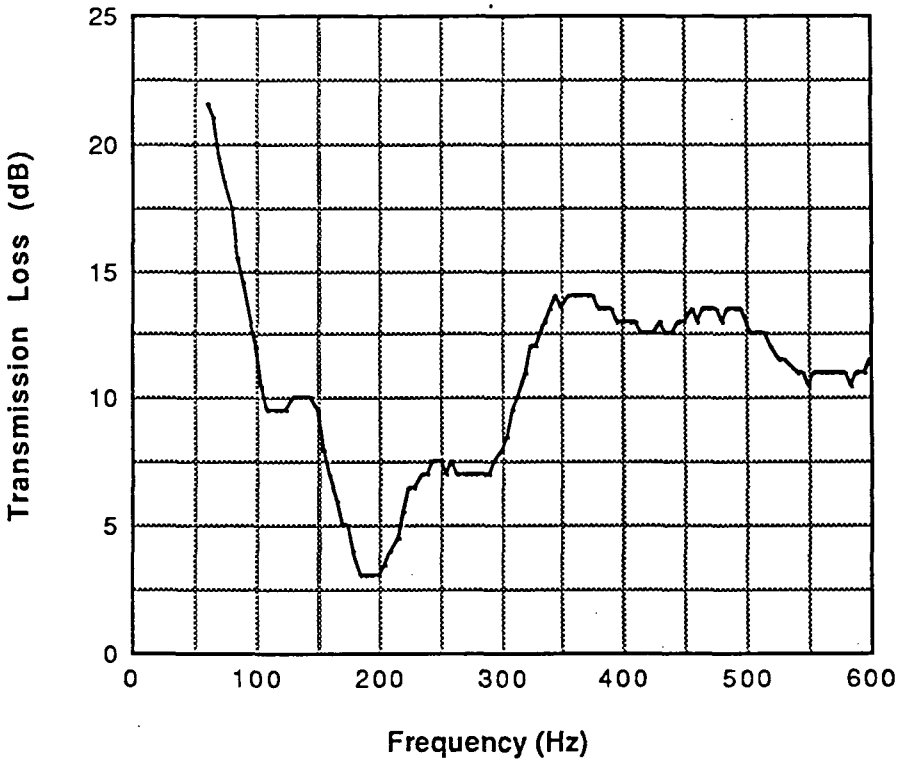

Figure 3c-7: Transmission loss data for the dual panel wall experiment with four identical speakers and the 1" coupling.

Next, the downstream panels were replaced with the same ART panels used in the initial experiment. Figure 3c-8 shows the transmission loss data with the two inch coupler in this configuration. There are three prominent minima: at 100 and 300 Hz, the resonances of the ART panels, and the coupling resonance minimum near 450 Hz. At the design frequency of 200 Hz, however, there is a transmission loss of 26 decibels. With the one inch coupler (Figure 3c-9), the same setup shows roughly the same results (note the coupling resonance minimum at 550 Hz).

Figures 3c-10, 3c-11, and 3c-12 show the improvements in transmission loss (ART result minus identical panel result) for the three couplers when the ART panels are used in the interior wall instead of identical panels. All three cases show dramatic transmission losses at the design frequency of 200 Hz, demonstrating that the ART concept works well in a dual-walled environment. Finally, figure 3c-13 shows the three previous curves overlaid, demonstrating that the size of the coupling gap has relatively little effect on the ART attenuation level and bandwidth.

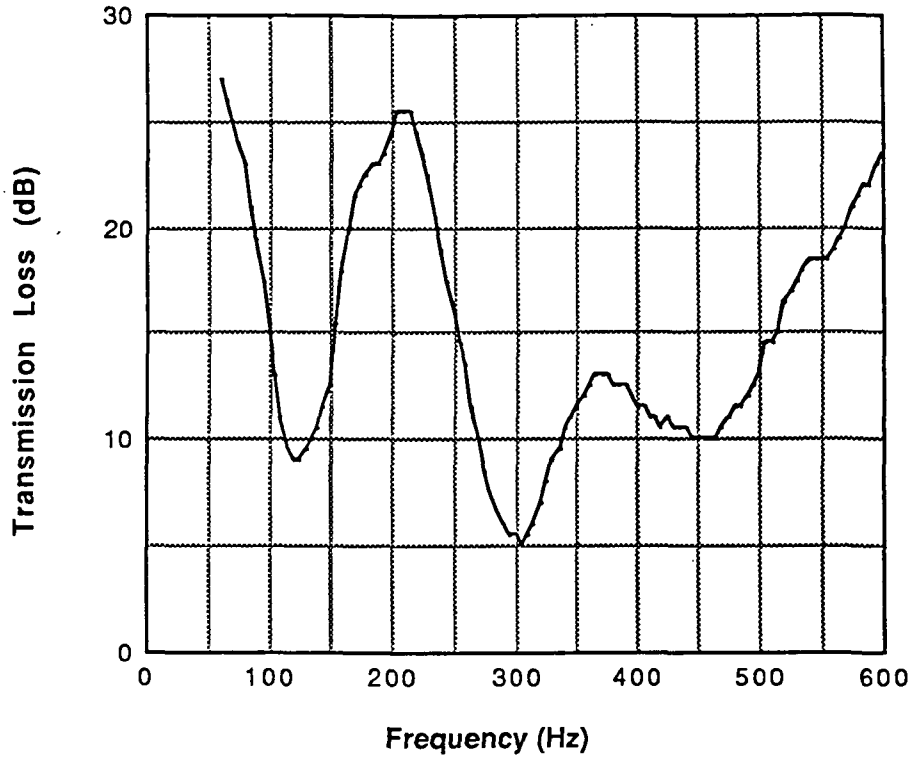

Figure 3c-8: Transmission loss data for the dual panel wall experiment with identical speakers upstream and ART speakers downstream.

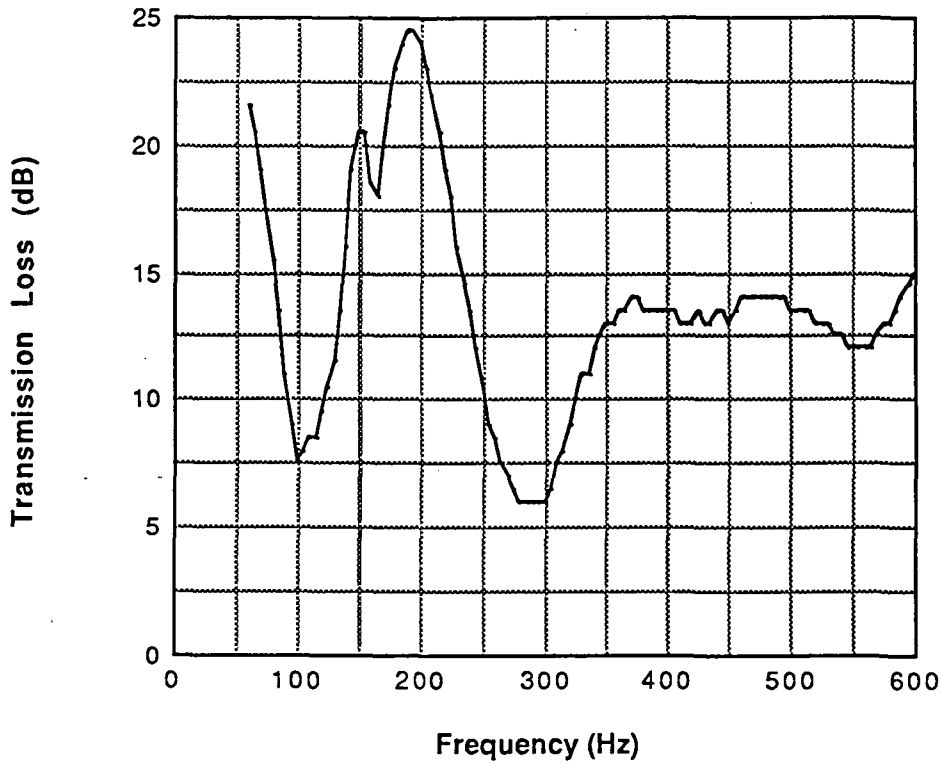

Figure 3c-9: Transmission loss data for the dual panel wall experiment with identical speakers upstream and ART speakers downstream with the 1" coupling.

Finally, it is noted that a corresponding set of experiments were conducted with the ART panels upstream and the identical panels downstream, simulating ART panels on the exterior fuselage wall. The results were very similar to those just presented, suggesting that the effectiveness of the ART concept is insensitive to whether it is applied on the interior or exterior wall.

Future work in this area will explore the application of ART panels on both the interior and exterior walls. The effect of small ART panels on one wall with large identical panels on the other will also be explored.

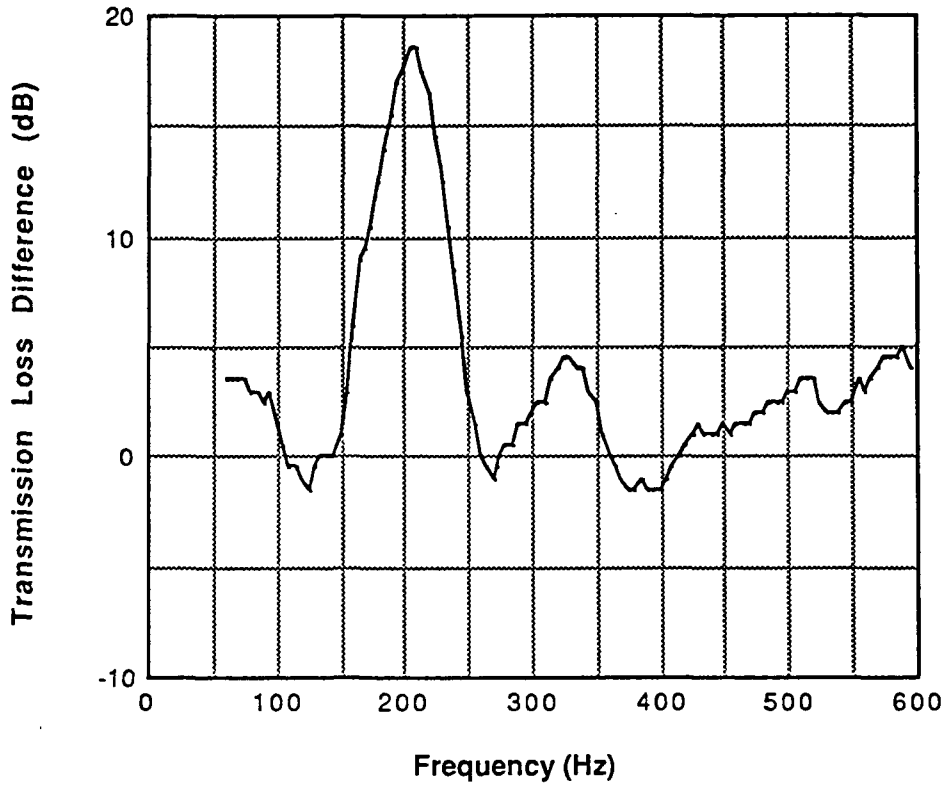

Figure 3c-10: Transmission loss difference between ART and identical speakers for the 7" coupling.

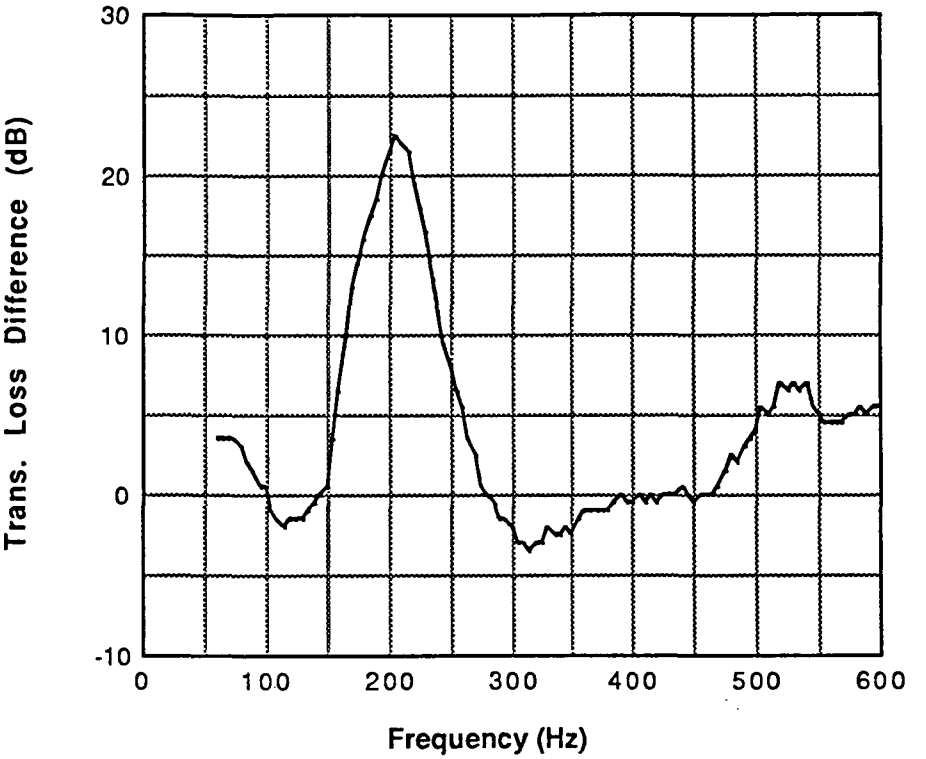

Figure 3c-11: Transmission loss difference between ART and identical speakers for the 2" coupling.

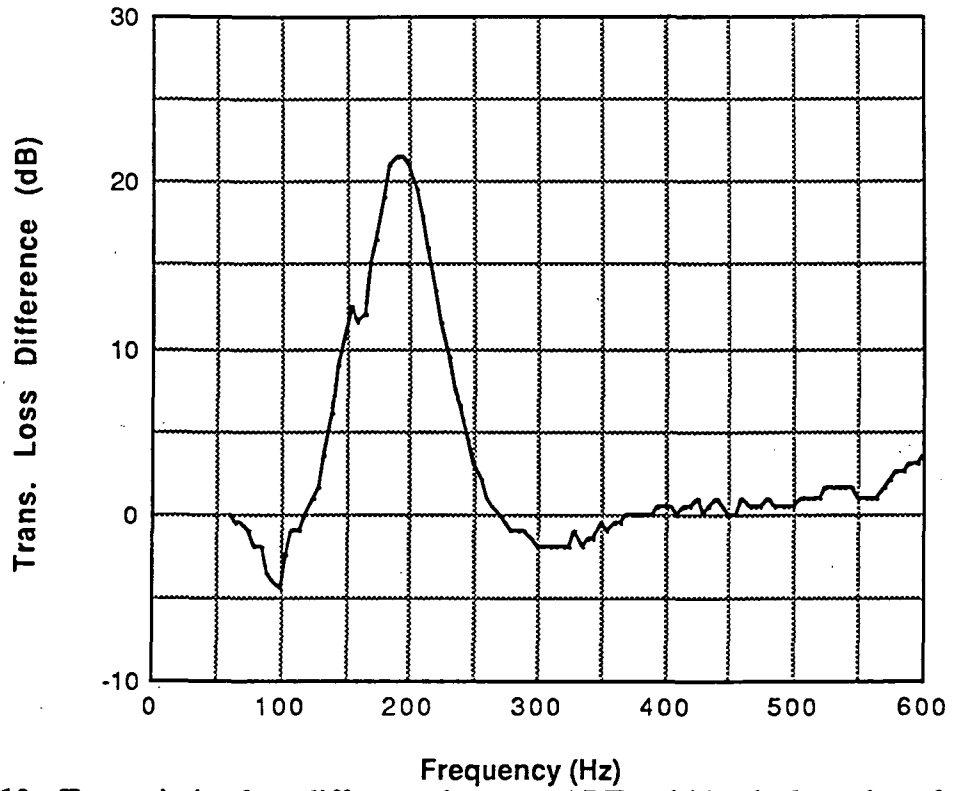

Figure 3c-12: Transmission loss difference between ART and identical speakers for the 1" coupling.

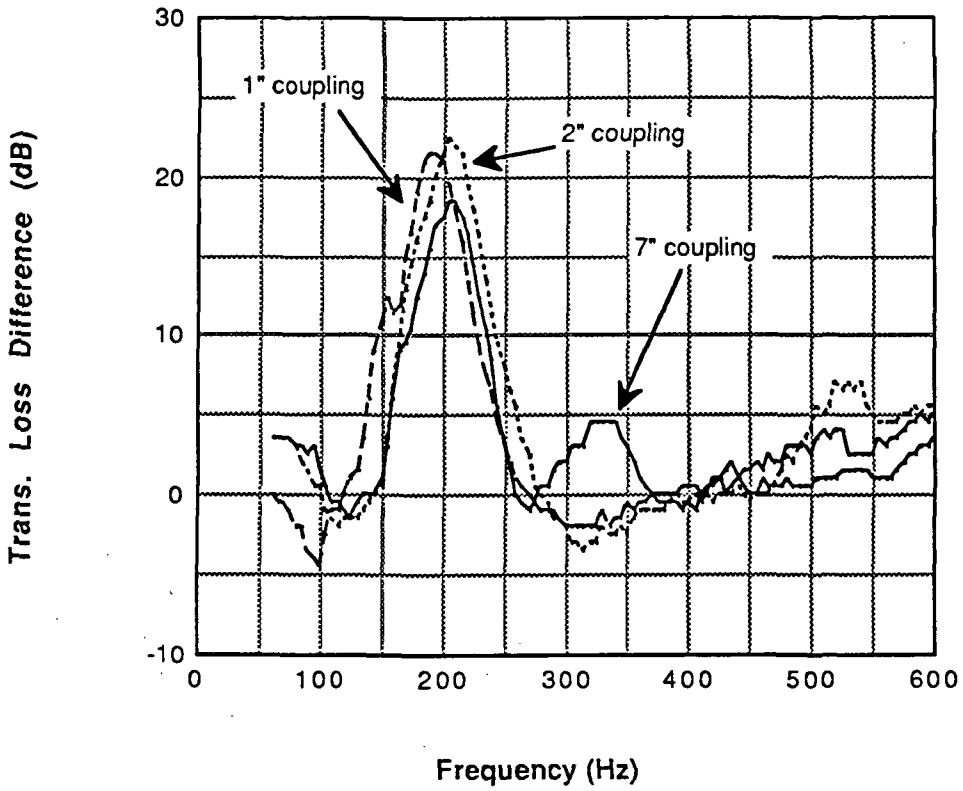

Figure 3c-13: Transmission loss difference between ART and identical speakers for the 7", 2", and 1" couplings.